Electronic Supplementary Material (ESI) for Nanoscale.

Electronic Supplementary Information

Etching-free patterning method for electrical characterizations of atomically thin CVD-grown $MoSe_2$ film

M. Iqbal Bakti Utama, Xin Lu, Da Zhan, Son Tung Ha, Yanwen Yuan,
Zexiang Shen and Qihua Xiong

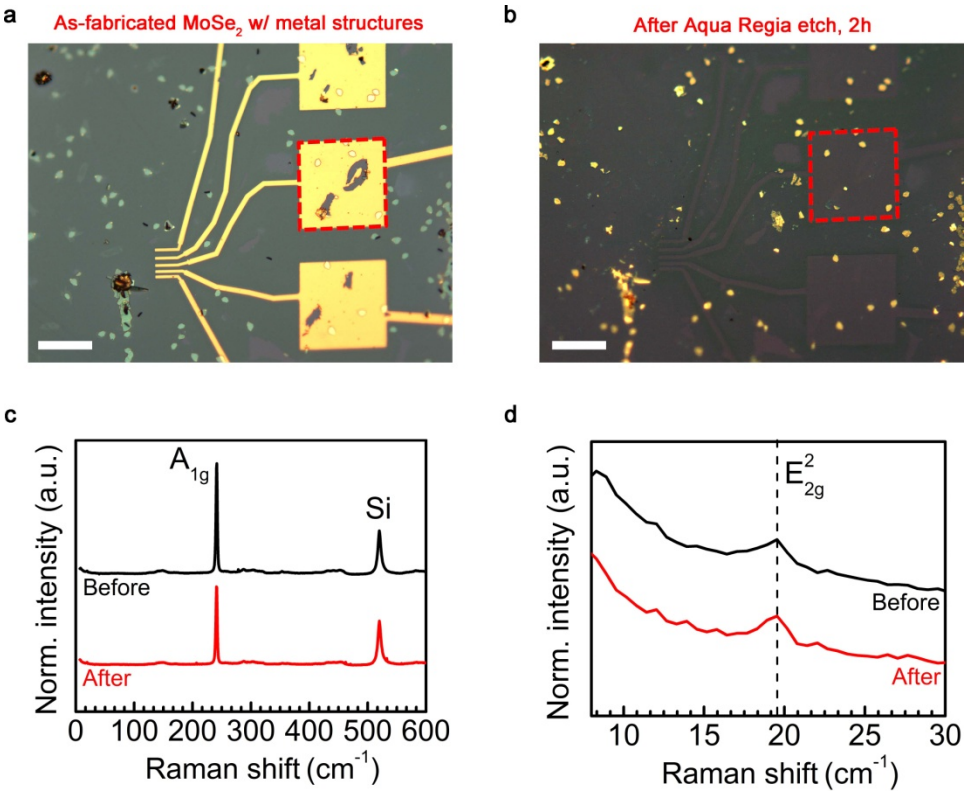

Fig. S1 Failure of Aqua Regia etching of $MoSe_2$ and the possibility of $MoSe_2$ patterning with metal sacrificial layer. (a,b) Optical micrograph of (a) Bilayer $MoSe_2$ film sample with metallic structures prior to etching, and (b) $MoSe_2$ sample after immersion in Aqua Regia for 2 hours. Dashed red squares on both micrographs denotes the same area. Scale bars in (a) and (b): 50 μm. (c) Raman spectra before and after Aqua Regia etching at an area not covered by metallic structures. (d) The same Raman spectra at the low frequency regime.

The etching rate of transition metal dichalcogenides (including $MoSe_2$) by commonly used wet etchant (*e.g.*, HCl, HNO_3, HF, KOH) is extremely low. The low wet etching rate creates impracticality to incorporate the method for lithography patterning of $MoSe_2$, since the etching rate of most organic etching mask is higher than that of $MoSe_2$. Fig. S1a and S1b shows the same area of $MoSe_2$ film before and after the immersion of the sample in undiluted Aqua Regia solution (HNO_3:HCl = 1:3) for 2 hours in room temperature, respectively. Prior to the etching, parts of the $MoSe_2$ film was covered by metallic patterns of 50 nm thick Ni metal deposited *via* lithography and thermal evaporation. The $MoSe_2$ film used herein is mostly comprised of monolayer and bilayer region. In addition, the $MoSe_2$ film also contains much thicker flakes, shown as blue notches in contrast to the dark-green hue of the film. After the Aqua Regia immersion, the Ni metal structures has disappeared completely (compare the dashed red square in Supplementary Fig. S3a and S3b). However, most of the thicker $MoSe_2$ flakes remained on the substrate. From the micrograph after the etching, it is still possible to distinguish the green hue of the remaining $MoSe_2$ film in contrast to the purple background originating from the uncovered SiO_2 substrate.

To elucidate further the ineffectiveness of Aqua Regia etching on $MoSe_2$, we compared the Raman spectra before and after the immersion of the sample (Fig. S1c). The Raman spectra were collected at identical condition with 532 nm laser excitation. After etching, the relative intensity of A_{1g} mode of $MoSe_2$ (241 cm^{-1}) is slightly reduced. However, the low frequency regime of the spectra showed that the position and the intensity of E^2_{2g} mode remained constant (Fig. S1d). As previously reported[1], the position of E^2_{2g} mode in $MoSe_2$ is strongly dependent on layer number: bilayer sample will exhibit peak at ~19 cm^{-1} whereas monolayer sample does not display the mode. This behavior is general in 2D TMD films; similar dependence of the position of low frequency Raman modes on the layer thickness has also been reported in details in MoS_2 and WSe_2 flakes[2,3]. The unchanging E^2_{2g} mode after the 2 hours etching indicates that Aqua Regia solution only slightly damages the $MoSe_2$ film without reducing the layer number yet.

Interestingly, the etching of the Ni structure also removes the $MoSe_2$ film beneath it, as seen by comparing Fig. S1a and S1b. The area that was previously covered by Ni is now purple-colored, which is the color of the SiO_2 substrate. We believe that the removal of $MoSe_2$ with the Ni—acting as a sacrificial layer—follows similar mechanism as the SU-8 patterning, which is due to stronger adhesion between Ni-$MoSe_2$ as compared to $MoSe_2$-SiO_2. We have also observed that similar patterning can also be accomplished with other metal sacrificial layer, such as Au, indicating that the choice of Ni is not unique.

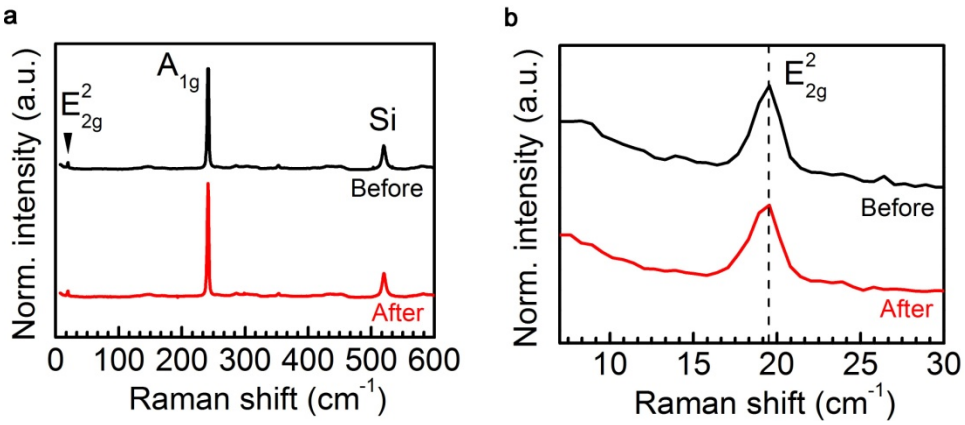

Fig. S2 Raman spectra on unpatterned $MoSe_2$. (a) Normalized Raman spectra (532 nm laser excitation) before and after SU-8 patterning process at $MoSe_2$ area that was unpatterned, *i.e.*, area whose SU-8 layer above it was unexposed by EBL. (b) The same Raman spectra at the low frequency regime. From (a) and (b), no significant changes were observed in intensity and wavenumber of all Raman modes. This provide an evidence that the optical properties of the sample were not affected by the patterning process.

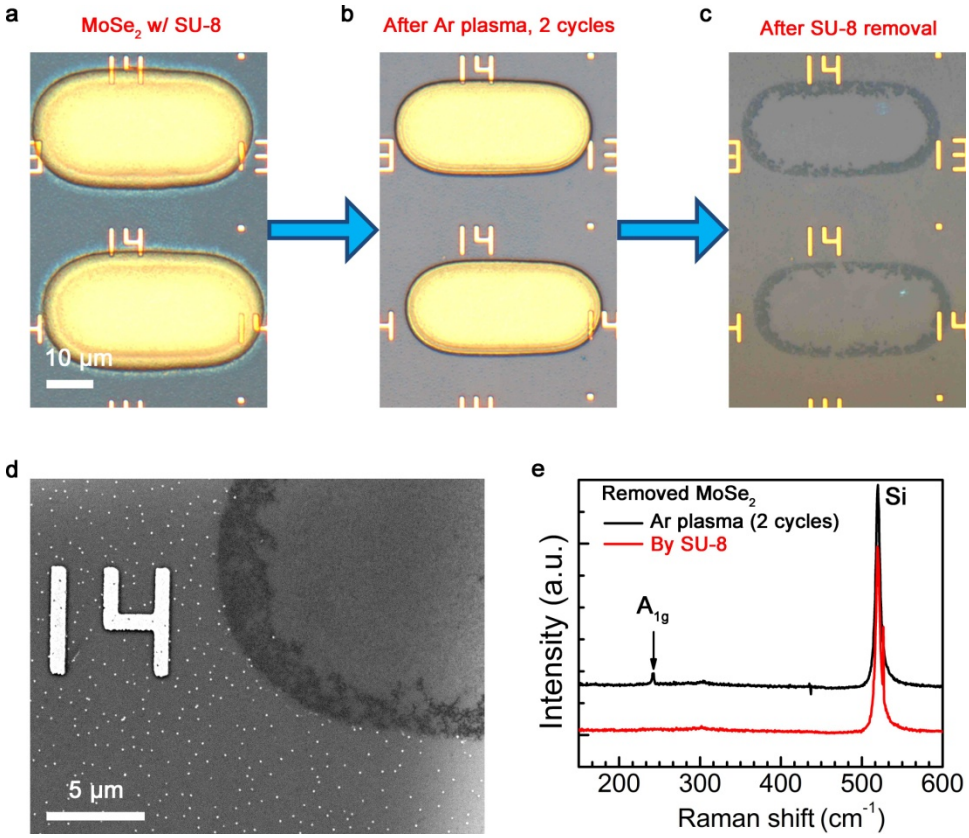

Fig. S3 Comparison of SU-8 patterning with Ar plasma etching. (a) Optical micrograph of $MoSe_2$ film sample with a developed SU-8 structure. The numbers are metal alignment marks deposited after the synthesis. Scale bar: 10 μm. (b) The same area after 2 cycles of Ar plasma (plasma surface treatment system; AST Products, 13.56 MHz RF source). Each cycle is conducted at 200 W plasma power, 10 Torr pressure, and room temperature, where each cycle lasts 5 min long. There is a perceptible change of the color of the sample area that is not covered by SU-8—from green tint to lighter purple—indicating that the etching had occurred on $MoSe_2$. Additionally, notice that the area of the SU-8 structure has shrunk as the Ar plasma etched the SU-8 as well. (c) The same area after the stripping of SU-8 layer in Remover PG. The $MoSe_2$ removal by SU-8 patterning was more thorough than that in the area etched by Ar plasma, which still contains numerous green particles. (d) Scanning electron micrograph of the sample, contrasting the removal result of $MoSe_2$ with Ar plasma etching and SU-8 patterning. Copious particles are evident on area that was Ar plasma-etched. Scale bar: 5 μm. (e) Raman spectra of the sample at the area etched by Ar plasma and that removed by SU-8. The area etched by Ar plasma does contain traces of $MoSe_2$, as indicated by a very weak A_{1g} peak. We conclude that SU-8 patterning removes 2D film more thoroughly than does dry etching that relies solely on sputtering mechanism, such as Ar plasma[4], which are prone to the redeposition of sputtered material.

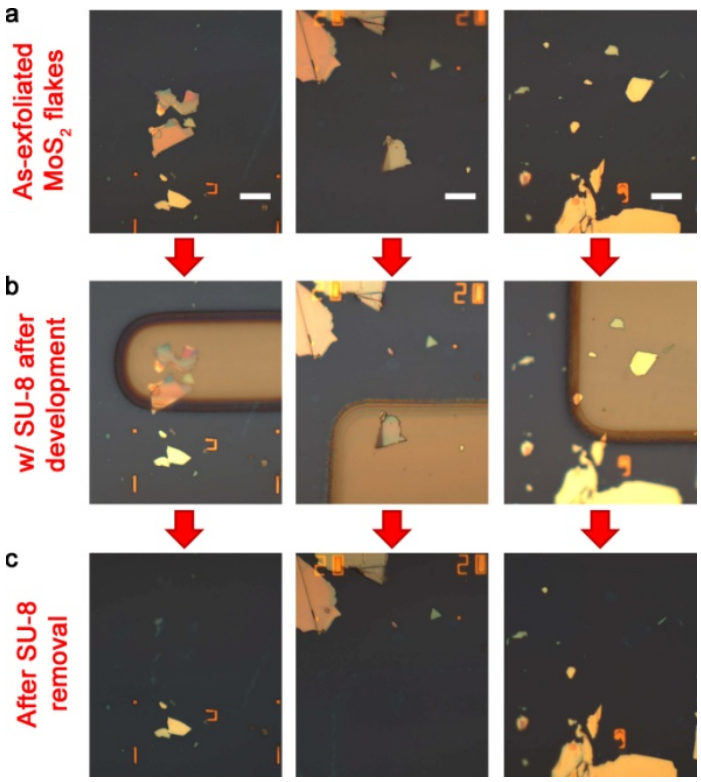

Fig. S4 Removal of exfoliated molybdenum disulfide (MoS_2) flakes with SU-8 patterning. (a) Optical micrographs of multilayer MoS_2 produced by scotch-tape exfoliation of geological bulk crystal (SPI Supplies) on 100 nm SiO_2 substrate containing Cr/Au marker patterns. All scale bars: 1 μm. (b) Micrograph of the same areas covered with exposed SU-8 after development process. The SU-8 processing follows the same procedure that was conducted on CVD-grown $MoSe_2$ film. (c) Micrograph of the same areas after the removal of SU-8 layer, thus removing the covered MoS_2 flakes as well. Similar to the case in CVD-grown $MoSe_2$ film, most of the flakes that are covered with exposed SU-8 layer are being removed from the substrate when the SU-8 structure is stripped by immersing the substrate in Remover PG solution. This experiment suggests that the SU-8 patterning is not limited to only $MoSe_2$ and sample produced with CVD. Nevertheless, we observed that the success yield of MoS_2 flakes removal with SU-8 is not as high as that of CVD-$MoSe_2$ removal, which suggests that the adhesion of a number of MoS_2 flakes on SiO_2 substrate is stronger than the typical adhesion of CVD-$MoSe_2$ film on SiO_2 substrate.

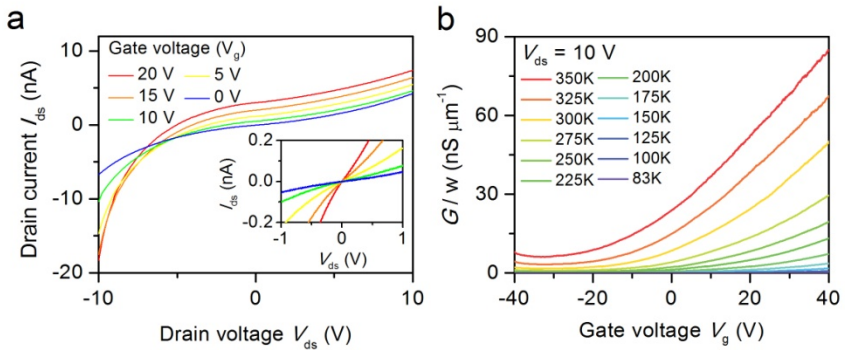

Fig. S5 Additional electrical characterization data on $MoSe_2$ devices. (a) I-V characteristics of unpatterned $MoSe_2$ device. The device exhibits $I_{ds} \neq 0$ A at $V_{ds} = 0$ V for $V_g \neq 0$ V, which implies that gate leak current is the primary contributor to the measured current. The gate leakage current obscures the device current that flows through the source and drain, making the output characteristics of the device not readily interpretable. *Inset:* I-V characteristics of the same device after SU-8 patterning of $MoSe_2$ film into a ribbon channel. After patterning, gate leakage has been suppressed and the drain current at all V_g intersects at $I_{ds} = 0$ A for $V_{ds} = 0$ V. The curves have also became nearly symmetrical for both polarity of the bias voltage. (b) Temperature dependence transfer curves of $MoSe_2$ device (Channel length: 10 μm). To calculate the field-effect mobility of the device[5,6], we use the formula $\mu = (\mathrm{d}I_{ds}/\mathrm{d}V_g) \times (L/WC_{ox}V_{ds})$, where L and W is the channel length and width of the device, and C_{ox} is the areal capacitance of the 100 nm gate oxide (3.45×10^{-4} F/m^2). The transconductance of the device $(\mathrm{d}I_{ds}/\mathrm{d}V_g)$ is calculated at the linear regime of the transfer curve.

Supplementary References

1 X. Lu, M. I. B. Utama, J. Lin, X. Gong, J. Zhang, Y. Zhao, S. T. Pantelides, J. Wang, Z. Dong, Z. Liu, W. Zhou and Q. Xiong, *Nano Lett.*, 2014, **14**, 2419-2425.

2 Y. Zhao, X. Luo, H. Li, J. Zhang, P. T. Araujo, C. K. Gan, J. Wu, H. Zhang, S. Y. Quek, M. S. Dresselhaus and Q. Xiong, *Nano Lett.*, 2013, **13**, 1007-1015.

3 X. Luo, Y. Zhao, J. Zhang, Q. Xiong and S. Y. Quek, *Phys. Rev. B*, 2013, **88**, 075320.

4 H. Nam, S. Wi, H. Rokni, M. Chen, G. Priessnitz, W. Lu and X. Liang, *ACS Nano*, 2013, **7**, 5870-5881.

5 A. Ayari, E. Cobas, O. Ogundadegbe and M. S. Fuhrer, *J. Appl. Phys.*, 2007, **101**, 014507.

6 B. Radisavljevic, A. Radenovic, J. Brivio, V. Giacometti and A. Kis, *Nature Nanotech.*, 2011, **6**, 147-150.